

Article

Electrodeposited Ni/TiN-SiC Nanocomposites on the Dumbbell: Reducing Sport Injuries

Haijun Bai * and Qiang Li

Department of Physical Education and Research, Heilongjiang Bayi Agricultural University, Daqing 163319, China; qiangli507@163.com

* Correspondence: haijliu2019@163.com; Tel.: +86-459-6502577

Abstract: Sports are becoming an important part of everyday life. In this study, an excellent Ni-SiC nanocomposite was prepared on the dumbbell surface using the pulse electrodeposition (PE) method to improve the durability of sports equipment and prevent sports injuries. Transmission electron microscopy (TEM), scanning electron microscopy (SEM), abrasion testing, triboindentation, and X-ray diffraction (XRD) were used to evaluate the impact of plating conditions upon the microhardness, microstructure, morphology, and wear behavior of the fabricated coatings. The obtained results showed that several SiC and TiN nanoparticles were incorporated into Ni/TiN-SiC nanocomposites obtained at 4 A/dm². SiC and TiN nanoparticles had mean diameters of 37.5 and 45.6 nm, respectively. The Ni/TiN-SiC nanocomposite produced at 4 A/dm² showed an excellent mean microhardness value of 848.5 HV, compared to the nanocomposites produced at 2 and 6 A/dm². The rate of wear for Ni/TiN-SiC nanocomposite produced at 4 A/dm² was 13.8 mg/min, demonstrating outstanding wearing resistance. Hence, it has been suggested that the Ni/TiN-SiC nanocomposite can effectively reduce sports injuries.

Keywords: Ni/TiN-SiC nanocomposite; dumbbell; pulse electrodeposition; wear resistance; microstructure



Citation: Bai, H.; Li, Q.

Electrodeposited Ni/TiN-SiC Nanocomposites on the Dumbbell: Reducing Sport Injuries. *Coatings* **2022**, *12*, 177. <https://doi.org/10.3390/coatings12020177>

Academic Editor: Paweł Nowak

Received: 18 December 2021

Accepted: 28 January 2022

Published: 30 January 2022

Publisher's Note: MDPI stays neutral with regard to jurisdictional claims in published maps and institutional affiliations.



Copyright: © 2022 by the authors. Licensee MDPI, Basel, Switzerland. This article is an open access article distributed under the terms and conditions of the Creative Commons Attribution (CC BY) license (<https://creativecommons.org/licenses/by/4.0/>).

1. Introduction

Sports have now become an integral element of human life. However, at the same time, the number of injuries caused by sports accidents during physical activities has risen dramatically [1–3]. Sports injuries can be minimized by using the proper equipment and keeping it in good condition. Hence, an excellent coating material can be used to cover the surface of sports equipment to prevent sports injuries and improve the durability of the equipment [4–6]. Nickel-based ceramic nanoparticle coating (NBCNC), a nanomaterial for enhancing the wear and corrosion resistance of sports equipment, is one of the most suitable and protective composite coatings for this equipment [7]. NBCNC also exhibited a high level of slip resistance, which is advantageous in decreasing sports injuries caused by hand slipping.

NBCNCs can be deposited in several different ways; electrodeposition, electroless plating, and brush plating are just a few of them. Electrodeposition methods provide several advantages over electroless and brush plating, including faster deposition speeds, lower costs, lesser electrode losses, and no restrictions on reinforcing particles [8–11]. Xu and colleagues [12] employed co-electrodeposition for the fabrication of SiC-Ni composites. Their findings indicated that the crystal size of the SiC-Ni coating was less than that of the monolayer Ni coating. The microstructure and characteristics of electrodeposited Ni-Mo/Al₂O₃ nanocomposites were investigated in detail by Alizadeh et al. [13]. They discovered that the nanocomposites had a considerable number of Al₂O₃ nanoparticles that were uniformly implanted. There are two types of electrodeposition processes: pulse current electrodeposition (PCE) and direct current electrodeposition (DCE) [14,15]. Lee

and colleagues [16] reported the successful prefabrication of boron nitride reinforced Ni-W nanocomposites through the PCE approach. PCE, in comparison with DCE, has been used in the chemical, military, mechanical, and petroleum industries due to its lower porosity and internal stress, increased plating rates, and refined matrix grains.

Ni/TiN-SiC nanocomposite is an NBCNC, comprising Ni grains, SiC, and TiN nanoparticles. SiC and TiN nanoparticles are high-performance inorganic ceramic materials. TiN nanoparticles, in particular, exhibit exceptional hardness and strength, as well as good resistance to corrosion and wear. As a result, TiN nanoparticles have been used as a reinforcing phase in the fabrication of coatings with superior physical and chemical attributes [17,18]. SiC nanoparticles, on the other hand, are more thermally stable, have a better slip and wear resistance, and have a high microhardness [19]. Several reports describing the deposition of Ni-TiN, Ni-SiC, and Cu-SiC coatings using PCE and DCE procedures have appeared recently. However, the PCE method for depositing Ni/TiN-SiC nanocomposites has only been investigated in a few studies. Thus, Ni/TiN-SiC nanocomposites were formed on sports equipment samples using PCE deposition to improve the composites' physical and chemical properties to minimize sports injuries. Furthermore, we conducted an extensive examination to determine the effect of plating parameters on the microstructure, morphology, microhardness, and wear behavior of Ni/TiN-SiC nanocomposites generated by PCE.

2. Experiment

Ni/TiN-SiC nanocomposites were synthesized on dumbbell samples using the PCE method using a modified plating solution comprising 28 g/L NiCl₂, 195 g/L NiSO₄, 28 g/L H₃BO₃, 70 mg/L cetyltrimethyl ammonium, 8 g/L TiN nanoparticles, and 8 g/L SiC nanoparticles. The diameters of SiC and TiN nanoparticles range from 30 to 40 nm. The anode was a pure nickel plate (120 mm × 40 mm × 20 mm), while a specimen of sporting equipment (Φ30 mm × 120 mm) served as the cathode. Between the two electrodes, a spacing of 180 mm was maintained. Figure 1 illustrates the experimental equipment used to synthesize Ni/TiN-SiC nanocomposites. The pulse current source (SMD-200, Handan Electroplating Factory, Handan, China), heating device, ultrasonic agitator (XIL-500, Beijing Xili Technology Co., LTD., Beijing, China), and plating bath were all included in the device. Pulse current densities of 2, 4, and 6 A/dm² were generated using a pulse current generator with a duty cycle of 40%. A heating system was used to maintain the plating solution at 45 °C. The ultrasonic agitator was used to maintain a uniform suspension of disseminated SiC and TiN nanoparticles within the solution of plating. The plating solution was adjusted to a pH of 4.7 by adding either sodium hydroxide (12 wt.%) or hydrochloric acid (15 vol.%), and the plating time was set to 40 min. The plating time was determined based on our previous study [7].

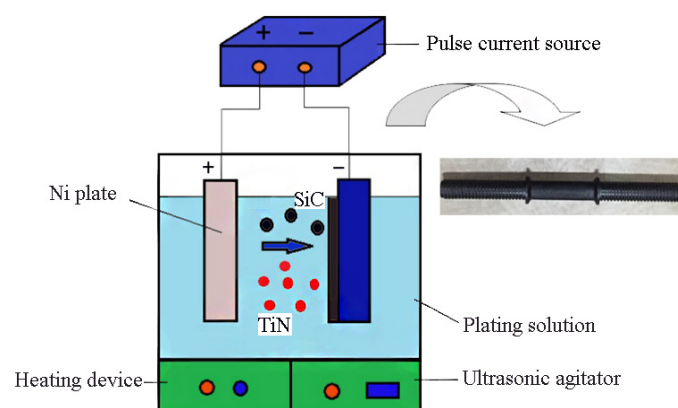


Figure 1. Experimental set-up for fabrication of Ni/TiN-SiC nanocoatings.

Scanning electron microscopy (SEM, S3400, Hitachi High-Tech Co., LTD., Tokyo, Japan) and IE-300X type energy dispersive spectroscopy (EDS) were used to study the morphological structures and cross-sections of the prepared Ni/TiN-SiC nanocomposites. The microstructures of Ni/TiN-SiC nanocomposites were surveyed via a Tecnai-G2-20 type transmission electron microscopy (TEM, FEI Co., LTD., Hillsboro, OR, USA). Firstly, the Ni/TiN-SiC samples were polished by using a PSY8120 type polishing machine (Suzhou Shengya Machinery Co., LTD., Suzhou, China), and then the samples were reduced by using a CSC-2000 type ion thinning meter (Shanghai Hezao Machinery Co., LTD., Shanghai, China). The main parameters of the TEM are as follows: acceleration voltage 200~300 kV, point resolution 0.2 nm, linear resolution 0.102 nm, and magnification 60~1000 k. Rigaku D/Max-2400 X-ray diffraction (XRD, Rigaku Co., LTD., Tokyo, Japan) with the radiation of Cu-K α ($k = 1.54$ nm) was carried out for determining the quantitative phase composition. The nanohardness of Ni/TiN-SiC nanocomposites was determined using a TI-950 triboincender (Berkovich indenter, Bruker Co., LTD., Billerica, MA, USA) with a force of loading of about 1000 μ N for 10 s. The MRH-6 abrasion tester was used to conduct friction and wear experiments on Ni/TiN-SiC nanocomposites to evaluate their wear parameters. To accomplish this, a hardened steel barrel (GC15) was slid across a nanocomposite surface at a constant speed of 0.1 m/s and 5 N applied load at room temperature. SEM was used to examine the worn surface morphologies of the Ni/TiN-SiC nanocomposites following 30 min of wear testing. The friction coefficient of the nanocomposite was acquired from the data collected via the abrasion tester. The wear rate of individual nanocomposite (V) was determined using Equation (1):

$$V = \frac{M1 - M2}{L} \quad (1)$$

Herein, $M1$ and $M2$ are the masses of individual samples before and after each wear test, respectively. The mass was determined using a lab balance. The sliding length of the hardened steel balls used in wear tests is indicated by the letter L .

3. Results and Discussion

3.1. SiC and TiN Nanoparticles

The morphological structures of the nanoparticles of SiC and TiN are shown in Figure 2. SiC and TiN nanoparticles were individually poured into an ethanol solution. Additionally, then they were dropped on a glass sheet. After a drying treatment, the glass sheets were tested by the TEM. Using the Nano Measurer 1.2 software, ten distinct SiC and TiN nanoparticles were measured, as shown in Figure 2a,b, respectively. According to the findings, the average diameters of SiC and TiN nanoparticles were 35 and 40 nm, respectively. These nanoparticles tend to agglomerate due to their surface effects. Additionally, in the microregions, regular crystal formations were manifested by SiC and TiN nanoparticles.

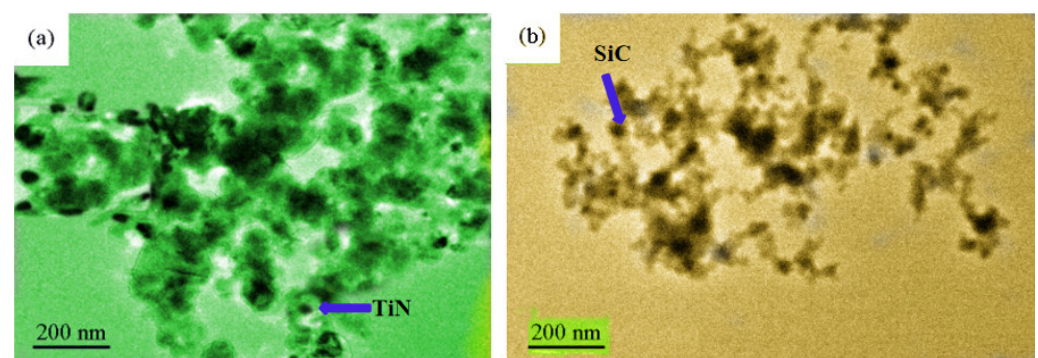


Figure 2. TEM micrographs for the products: (a) TiN, and (b) SiC nanoparticles.

3.2. SEM Analysis

The SEM-based surface morphological features of Ni/TiN-SiC nanocomposites synthesized at pulse current densities of 2, 4, and 6 A/dm², as shown in Figure 3a–c. Figure 3a'–c' represents the corresponding Ni/TiN-SiC nanocomposites in terms of their cross-section morphologies. The pulse current density has a significant influence on the surface morphologies of Ni/TiN-SiC nanocomposites. At a density of 2 A/dm², a Ni/TiN-SiC coating developed many large granular formations with an uneven and rough structure. SEM observations revealed Ni/TiN-SiC nanocomposites with smooth, homogeneous, and finer surface morphologies at an elevated pulse current density of 4 A/dm². However, at 6 A/dm² pulse current density, the grain sizes of Ni/TiN-SiC nanocomposites grew larger in comparison to those produced at 4 A/dm². Sajjadnejad and coworkers [20] stated that electroplating parameters, for instance duty cycle, pulse current density, and pulse frequency, are capable of influencing the microstructures of nickel-based coatings. According to their results, pulse current density can effectively refine grain size. However, an excessive pulse current density (e.g., 6 A/dm²) resulted in a significant amount of hydrogen being produced on the cathode surface, which prevented the deposition of SiC and TiN nanoparticles on the coating surface. The underlined process resulted in a rapid growth rate of nickel grains in the coatings. Additionally, an increment in the pulse current density from 2 to 6 A/dm², resulted in an increase in the thickness of Ni/TiN-SiC nanocomposites from 46.6 μm to 58.5 μm (Figure 3a'–c'), illustrating the influence of pulse current density upon the rate of deposition for the whole nanocomposite [21].

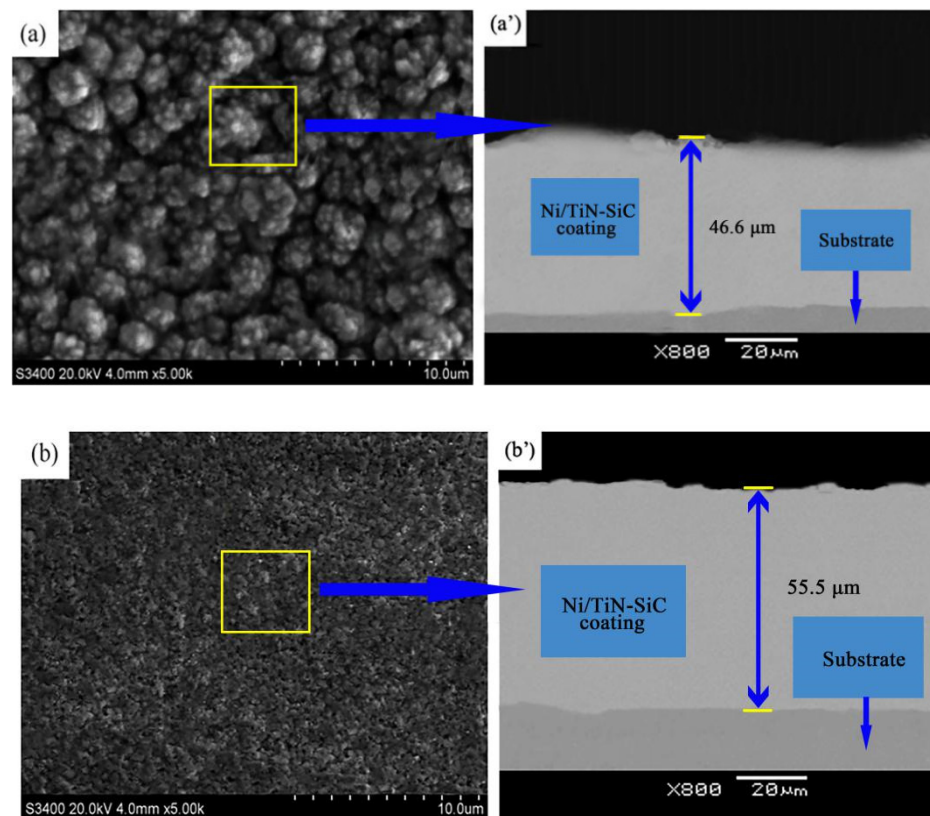


Figure 3. Cont.

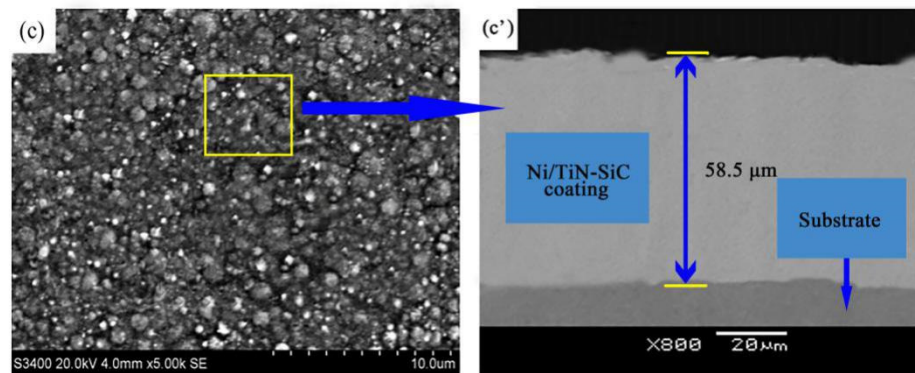


Figure 3. SEM micrographs of Ni/TiN-SiC nanocomposites fabricated by employing various pulse current densities: (a) and (a') 2 A/dm², (b) and (b') 4 A/dm², and (c) and (c') 6 A/dm².

3.3. TEM

Figure 4 demonstrates the micrographs of TEM for Ni/TiN-SiC nanocomposites generated as a function of diverse pulse current densities. In Figure 4a–c, the black parts depict SiC and TiN nanoparticles, while nickel grains are depicted by the white regions. Some SiC and TiN nanoparticles were observed on the Ni/TiN-SiC nanocomposite deposited at 2 A/dm², whereas multiple SiC and TiN nanoparticles were incorporated at 4 A/dm². SiC and TiN nanoparticles were found to have average sizes of 45.6 and 37.5 nm, respectively. This could presumably be a consequence of the moderate pulse current density, resulting in a large number of SiC and TiN nanoparticles embedded into the Ni/TiN-SiC nanocomposite. This result produced an effective inhibition of the growth of nickel grains. Nevertheless, the Ni/TiN-SiC nanocomposite deposited at 6 A/dm² processed comparatively large nickel grains with a small amount of SiC and TiN nanoparticles. The reason for this can be explained by the fact that the high pulse current density produced a large amount of hydrogen on the cathode surface, limiting the deposition of SiC and TiN nanoparticles on the coating surface. As a result, the nickel granules in the coatings expanded rapidly, but the SiC and TiN content remained low.

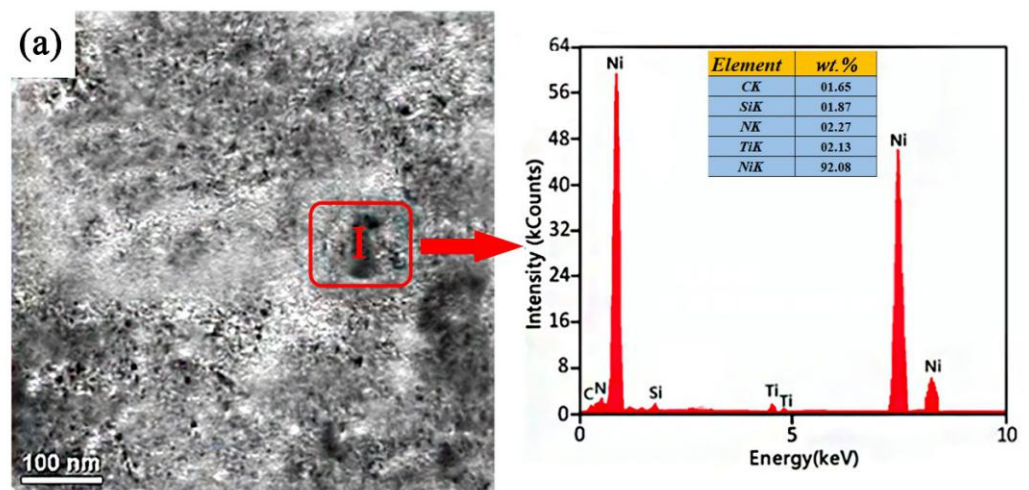


Figure 4. Cont.

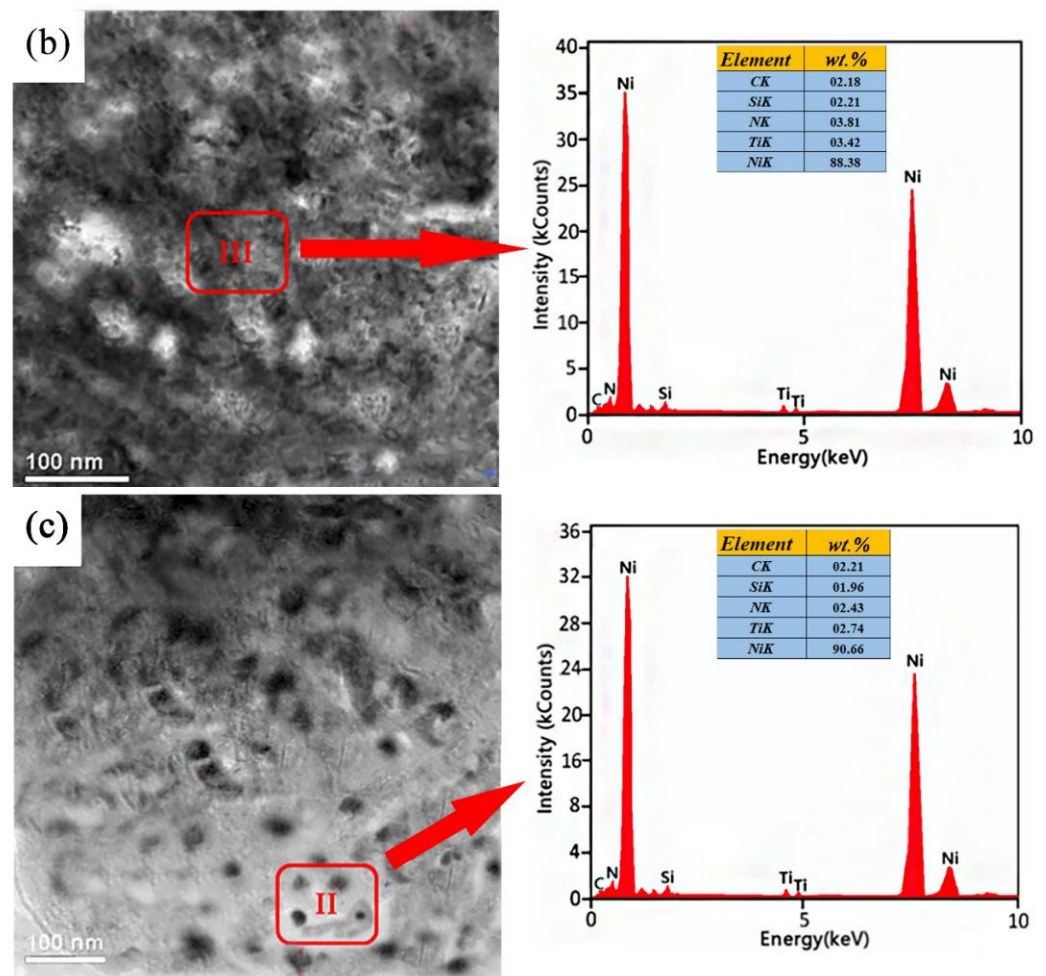


Figure 4. Micrographs of TEM for Ni/TiN-SiC nanocomposites fabricated using various current densities: (a) 2 A/dm², (b) 4 A/dm², and (c) 6 A/dm².

3.4. Codeposition Mechanism

The co-deposition of Ni ions, SiC, and TiN nanoparticles in the PCE is indicated in Figure 5, which is consistent with Guglielmi's hypothesis. The Ni ions present in the plating solution initially adsorb onto the surfaces of SiC and TiN nanoparticles. Following that, several ion clouds formed and suspended themselves within the bath. The nickel ions, SiC, and TiN nanoparticles migrated toward the cathode surface under the influence of the electric field force (F). Simultaneously, hydrogen formed on the cathode's surface. SiC and TiN nanoparticles were able to penetrate both the hydrogen evolution layer and the electric double layer and co-deposit on the cathode surface with Ni grains. With increasing deposition time, large numbers of nickel grains completely encapsulated SiC and TiN nanoparticles, resulting in the formation of the Ni/TiN-SiC nanocomposite.

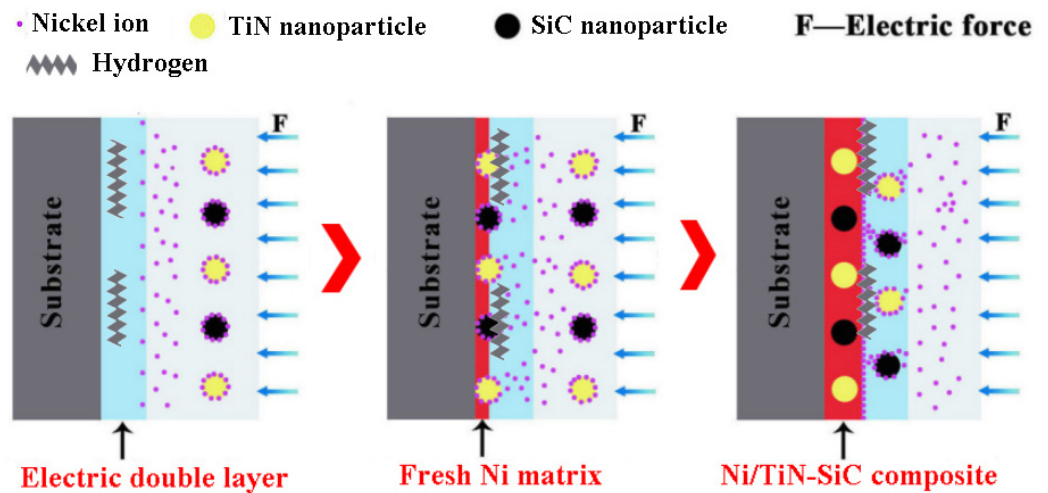


Figure 5. The mechanism of co-deposition for the nickel ions, SiC, and TiN nanoparticles.

Pulse current density also had a significant effect on the distribution and amount of SiC and TiN nanoparticles embedded in Ni/TiN-SiC nanocomposites [22]. Equation (2) revealed the link between pulse current density and electric field force.

$$F = \frac{I \times q}{\sigma} \quad (2)$$

Herein, the I represents pulse current density, q denotes the ion charge, and σ represents the conductivity of the solution.

The influence of electric field forces on SiC and TiN nanoparticles in the course of PCE deposition of Ni/TiN-SiC nanocomposites was not noticeable at lower pulse current densities (e.g., 2 A/dm²), resulting in rather limited incorporation of SiC and TiN nanoparticles within the coating. As a result, SiC and TiN nanoparticles did not affect nickel grain growth, allowing for unfettered nickel grain growth and the creation of multiple nickel grains with an average size of 96.4 nm (see Figure 4a).

Appropriate pulse current densities (e.g., 4 A/dm²), on the other hand, can significantly accelerate the rates of SiC and TiN nanoparticles towards the cathode, resulting in significant SiC and TiN nanoparticle incorporation into Ni/TiN-SiC nanocomposite. As a result, TiN and SiC nanoparticles provided a large number of nuclei for Ni grain formation while limiting Ni grain growth, resulting in uniform, smooth, and fine morphologies for Ni/TiN-SiC nanocomposites. The average size of nickel grains was ~74.3 nm, and the amounts of TiN and SiC nanoparticles in the nanocoating were 7.23 and 4.39 wt.%, as shown in Figure 4b. Furthermore, with a pulse current density of 6 A/dm², considerable numbers of hydrogen bubbles form at the cathode's surface, increasing the thickness of the layer of hydrogen formation. As a result, the deposition of SiC and TiN nanoparticles upon the surface of the cathode was hampered, resulting in a lower concentration of embedded SiC and TiN nanoparticles within Ni/TiN-SiC nanocomposites. Nickel granules' inhibitory action was also reduced, resulting in a larger grain size of 82.7 nm (see Figure 4c).

3.5. Phase Structure

Figure 6 illustrates the patterns of XRD for Ni/TiN-SiC nanocomposites fabricated at various pulse current densities. All the Ni/TiN-SiC nanocomposites achieved at 2 A/dm², 4 A/dm², and 6 A/dm² showed the existence of Ni, SiC, and TiN phases. For Ni grains, a set of three strong diffraction peaks were seen at 44.8°, 52.2°, and 76.7°, corresponding to (1 1 1), (2 0 0), and (2 2 0) planes, respectively. This result indicated that the Ni phase was face-centered cubic, which would be typical for Ni. Three strong diffractions at 34.1°, 41.6°, and 59.7° were detected in the case of SiC nanoparticles and were ascribed to the (1 1 1), (2 0 0), and (2 2 0) planes, respectively. Three significant diffraction patterns were seen for

TiN nanoparticles at 36.6° , 42.6° , and 61.8° , which were attributed to the (1 1 1), (2 0 0), and (2 2 0) planes, respectively.

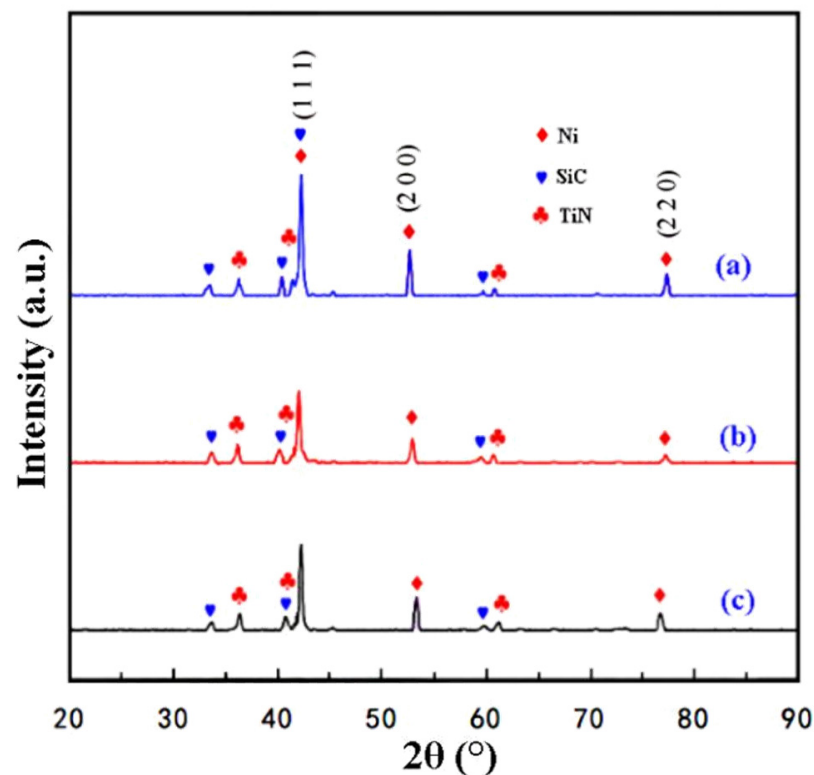


Figure 6. XRD patterns for Ni/TiN-SiC nanocomposites prepared using diverse pulse current densities: (a) 2 A/dm^2 , (b) 4 A/dm^2 , and (c) 6 A/dm^2 .

3.6. Microhardness Assessment

Figure 7 shows the impact of pulse current density upon the microhardness of the deposited Ni/TiN-SiC nanocomposites. The Ni/TiN-SiC nanocomposites were cut using a DK775 type electrical discharge cutting machine (Changfeng Cutting Machine Co., LTD., Taizhou, Jiangsu, China). Following that, the samples were polished with a polishing machine. The triboindenter was used to determine the microhardness of the coating over the sample's cross-section. The Ni/TiN-SiC nanocomposite deposited at 4 A/dm^2 had the highest microhardness of all the nanocomposites, with a mean microhardness of 848.5 HV. In comparison, the average microhardness of the Ni/TiN-SiC nanocomposite produced at 2 A/dm^2 was only 698.7 HV. However, the Ni/TiN-SiC nanocomposite obtained at 6 A/dm^2 has an average microhardness of 801.2 HV. According to previously reported studies [23,24], the microhardness of metal-based composites should be determined not only by the amount of SiC and TiN nanoparticles, but also by their distribution within the coating. SiC and TiN nanoparticles were abundant and distributed uniformly in Ni/TiN-SiC nanocomposites produced at 4 A/dm^2 , resulting in high microhardness and a dispersion-hardening effect. Furthermore, SiC and TiN nanoparticles each had individual microhardness values, enhancing the microhardness of the composites.

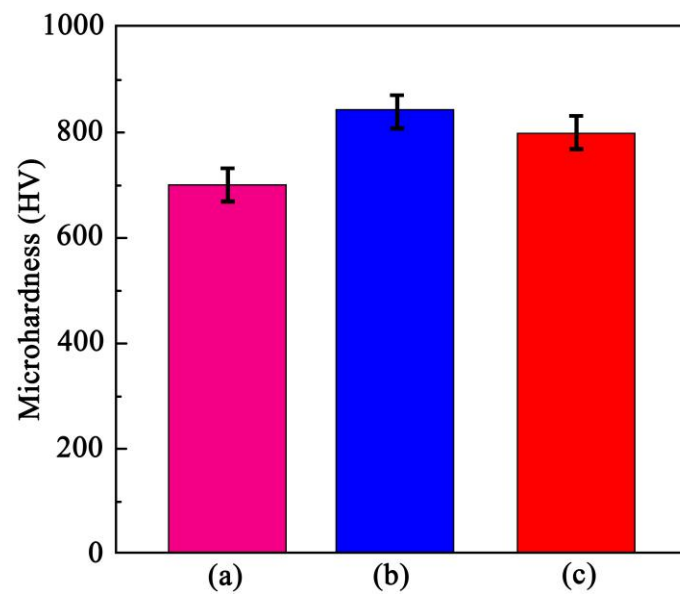


Figure 7. Influence of pulse current density on microhardness for Ni/TiN-SiC nanocomposites. (a) Composite obtained at 2 A/dm², (b) Composite obtained at 4 A/dm², and (c) Composite obtained at 6 A/dm².

3.7. Wear Assessment

3.7.1. Wear Rate

Figure 8 illustrates the wear rates of Ni/TiN-SiC nanocomposites deposited at various pulse current densities. During wear testing, the wear rates were gathered each 5 min, and then every two points were interconnected with a straight line. The greatest rate of wear for a Ni/TiN-SiC nanocomposite produced at 2 A/dm² was 27.1 mg/min, as shown in Figure 8a. Nonetheless, the rate of wear for a Ni/TiN-SiC nanocomposite formed at 4 A/dm² was as low as 13.8 mg/min (see Figure 8b), illustrating the high wear resistance of Ni/TiN-SiC nanocomposites.

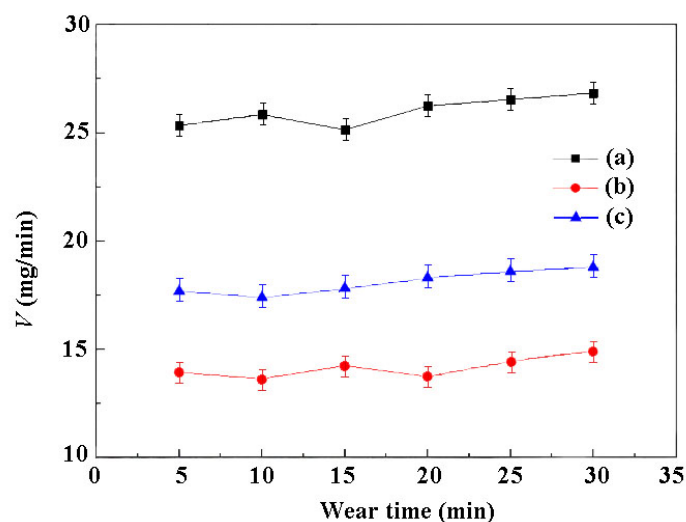


Figure 8. Wear rates of Ni/TiN-SiC nanocomposites generated with diverse pulse current densities: (a) 2 A/dm², (b) 4 A/dm², and (c) 6 A/dm².

3.7.2. Worn Surface Morphology

The morphologies of the worn surface for Ni/TiN-SiC nanocomposites formed at various pulse current densities are shown in Figure 9. On the worn surfaces of Ni/TiN-SiC nanocomposite deposited at 2 A/dm^2 , numerous deep grooves and pits developed, revealing a nanocomposite surface with a substantial wear state. However, only slight scratches were visible on the nanocomposite surface when applied at 4 A/dm^2 , demonstrating greater wear resistance. On the other hand, pulse current densities of approximately 6 A/dm^2 generated some large-scale grooves on the nanocomposite surface.

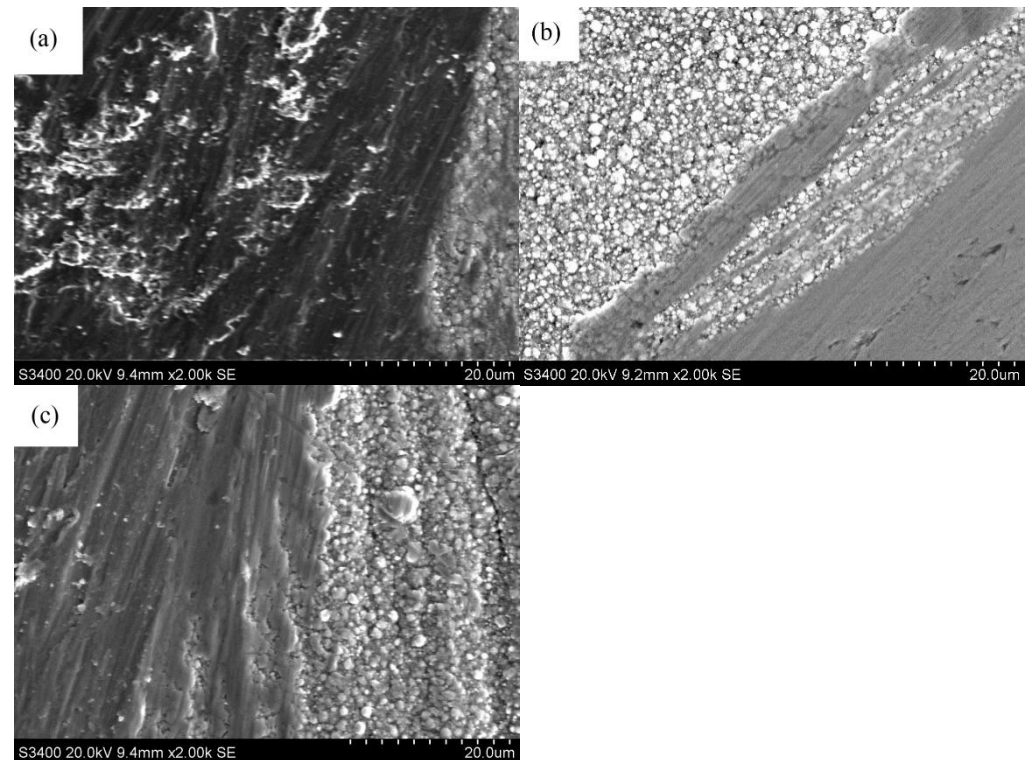


Figure 9. Micrographs of SEM for the worn surfaces of Ni/TiN-SiC nanocomposites generated using various pulse current densities: (a) 2 A/dm^2 , (b) 4 A/dm^2 , and (c) 6 A/dm^2 .

3.7.3. Friction Coefficient

Figure 10 shows the curves of the friction coefficient for Ni/TiN-SiC nanocomposites deposited at various pulse current densities. The friction coefficients of all Ni/TiN-SiC nanocomposites increased substantially for the first five minutes of the wear test. Among the three coatings, the composite formed at 2 A/dm^2 processed the highest friction coefficient. As the uneven surface caused the steel barrel to vibrate violently up and down, the friction coefficient changed dramatically. When the wear period was increased from 5 to 30 min, the Ni/TiN-SiC nanocomposite formed at 4 A/dm^2 had the lowest mean coefficient of friction of all three nanocomposites, around 0.48. The mean friction coefficient of the nanocomposite deposited at 2 A/dm^2 was 0.77. The amount of SiC and TiN nanoparticles in the composite, as well as its microhardness, are the critical characteristics that govern the friction coefficient of Ni/TiN-SiC nanocomposites [25]. During wear tests, several SiC and TiN nanoparticles were detached from the nickel matrix as the nickel grains were worn out. This phenomenon was reported by Mousavian et al. [26]. The friction coefficient was lowered by changing the mode of friction between the steel barrel and the Ni/TiN-SiC nanocomposite from sliding to rolling.

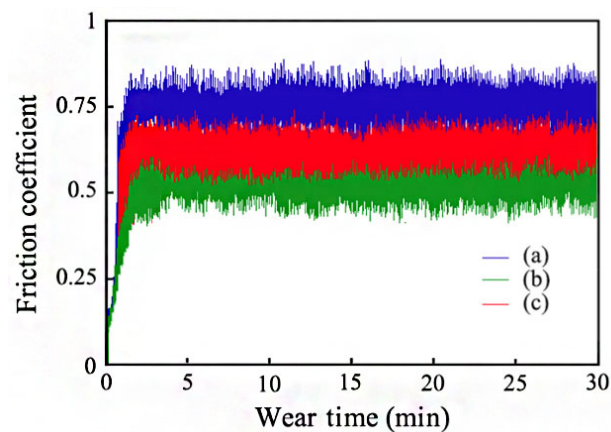


Figure 10. Coefficients of friction for Ni/TiN-SiC nanocomposites generated with diverse pulse current densities: (a) 2 A/dm², (b) 4 A/dm², and (c) 6 A/dm².

3.8. Application

To reduce the above-mentioned sports injuries and improve the durability of sports equipment, the Ni/TiN-SiC nanocomposite obtained at 4 A/dm² was prepared on the surface of a B20-1 type dumbbell, as shown in Figure 11. Figure 11a presents the dumbbell covered with many rusts (denoted as B20-1-A), and it was found that that the dumbbell's grip had a coarse surface, making it easier to harm our hands. Figure 11b is the barbell coated with Ni/TiN-SiC nanocomposite on its handle (denoted as B20-1-B). It indicated a smooth and compact surface, which was conducive to reducing sports injuries.

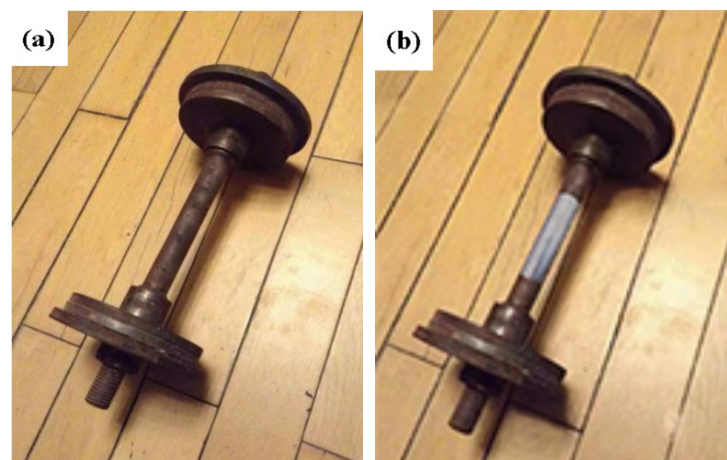


Figure 11. Images of the B20-1-A (a) and B20-1-B (b) dumbbells.

To determine the application effect of the two dumbbells, we elevated them 20 times per day for a total of seven days. Table 1 summarizes the number of injuries.

Table 1. The number of injuries for B20-1-A and B20-1-B dumbbells during this experiment.

Day	Number of Injuries (B20-1-A)	Number of Injuries (B20-1-B)
1	11	0
2	9	1
3	7	0
4	7	0
5	6	1
6	5	0
7	6	0
Total	51	2

The number of injuries occurred 51 times each week when we raised the B20-1-A dumbbell. The reason for this was that the rust on the surface of the B20-1-A dumbbell posed a risk of injury to our hands. However, when we raised the B20-1-B dumbbell, we experienced only two injuries each week as a result of an abrupt slide. In this view, the Ni/TiN-SiC nanocomposite has the potential to significantly minimize sports-related injuries.

4. Conclusions

(1) The SEM data revealed smooth, homogeneous, and fine surface morphological attributes of the Ni/TiN-SiC nanocomposites at a pulse current density of 4 A/dm². While some TiN and SiC nanoparticles appeared in the Ni/TiN-SiC nanocomposite deposited at 2 A/dm². Furthermore, the majority of SiC and TiN nanoparticles are integrated at 4 A/dm². The mean diameters of SiC and TiN nanoparticles are 37.5 and 45.6 nm, respectively. However, at 6 A/dm² pulse current density, the grain sizes of Ni/TiN-SiC nanocomposites were larger in comparison to those produced at 4 A/dm².

(2) In Ni/TiN-SiC nanocomposites produced at 2, 4, and 6 A/dm², Ni, TiN, and SiC phases were all present. There were fewer SiC and TiN nanoparticles within the Ni/TiN-SiC nanocomposite synthesized at 2 A/dm² in comparison to those fabricated at 4 A/dm² and 6 A/dm². However, with a pulse current density of 6 A/dm², considerable numbers of hydrogen bubbles form at the cathode's surface, increasing the thickness of the layer of hydrogen evolution. SiC and TiN nanoparticle deposition on the cathode surface was inhibited, resulting in a decreased concentration of embedded SiC and TiN nanoparticles within Ni/TiN-SiC nanocomposites.

(3) With a mean microhardness of 848.5 HV, the Ni/TiN-SiC nanocomposite deposited at a current density of 4 A/dm² had the highest microhardness of the nanocomposites. In comparison, Ni/TiN-SiC nanocomposite produced at 2 A/dm² manifested a mean microhardness as low as 698.7 HV. However, the Ni/TiN-SiC nanocomposite obtained at 6 A/dm² processed an average microhardness of 801.2 HV.

(4) The Ni/TiN-SiC nanocomposite generated at 4 A/dm² had a wear rate as low as 13.8 mg/min, demonstrating good wear resistance. Furthermore, the Ni/TiN-SiC nanocomposite prepared at 4 A/dm² had the lowest value of mean friction coefficient (0.48). The nanocomposite deposited at a current density of 2 A/dm² exhibited the largest value of the mean coefficient of friction, with a value equivalent to 0.77.

(5) It was found that when we lifted the B20-1-A dumbbell, 51 injuries occurred per week. However, when we raised the B20-1-B dumbbell, we saw only two injuries each week as a result of an abrupt slide. As a result, the Ni/TiN-SiC nanocomposite has the potential to significantly minimize sports-related injuries.

Author Contributions: Conceptualization and investigation, writing—review, H.B.; writing—original draft preparation, Q.L. All authors have read and agreed to the published version of the manuscript.

Funding: This work has been supported by the Heilongjiang Bayi Agricultural University Support Program for San Heng San Zong (Granted No. TDJH202005), and the Scientific Research Starting Foundation for Returnees and Excellent Scholars (Granted No. XDB201804).

Institutional Review Board Statement: Not applicable.

Informed Consent Statement: Not applicable.

Data Availability Statement: Not applicable.

Conflicts of Interest: The authors declare that they have no known competing financial interest or personal relationship that could have appeared to influence the work reported in this paper.

References

1. Elliott, J.; Heron, N.; Versteegh, T.; Gilchrist, I.A.; Peek, K. Injury reduction programs for reducing the incidence of sport-related head and neck injuries including concussion: A systematic review. *Sports Med.* **2021**, *51*, 17–23. [[CrossRef](#)] [[PubMed](#)]
2. Martin, T.G.; Wallace, J.; Suh, Y.I.; Harriell, K.; Tatman, J. Sport-related-concussions pilot study: Athletic training students media use and perceptions of media coverage. *Int. J. Sport Commun.* **2018**, *11*, 75–94. [[CrossRef](#)]

3. Song, H.; Han, X.Y.; Montenegro-Marin, C.E.; Krishnamoorthy, S. Secure prediction and assessment of sports injuries using deep learning based convolutional neural network. *J. Ambient. Intell. Humaniz. Comput.* **2021**, *12*, 3399–3410. [[CrossRef](#)]
4. Porac, C. Hand preference and the incidence of accidental unilateral hand injury. *Neuropsychologia* **1993**, *31*, 355–362. [[CrossRef](#)]
5. Martin, C.L.; Shanley, E.; Harnish, C.; Knab, A.; Christopher, S.; Vallabhajosula, S.; Bullock, G. The relationship between flourishing, injury status, and resilience in collegiate athletes. *Int. J. Sports Sci. Coach.* **2021**, *16*, 925–933. [[CrossRef](#)]
6. Mckinney, A.M.; Thompson, L.R.; Truwit, C.L.; Velders, S.; Karagulle, A.; Kiragu, A. Unilateral hypoxic-ischemic injury in young children from abusive head trauma, lacking craniocervical vascular dissection or cord injury. *Pediatr. Radiol.* **2008**, *38*, 164–174. [[CrossRef](#)] [[PubMed](#)]
7. Xia, F.; Li, C.; Ma, C.; Li, Q.; Xing, H. Effect of pulse current density on microstructure and wear property of Ni-TiN nanocoatings deposited via pulse electrodeposition. *Appl. Surf. Sci.* **2021**, *538*, 148139. [[CrossRef](#)]
8. Zhou, H.; Wang, W.; Gu, Y.; Fang, X.; Bai, Y. Study on the fabrication of Nano-SiC/Ni-P composite coatings with the assistance of electromagnetic-ultrasonic compound field. *Strength Mater.* **2017**, *49*, 101–108. [[CrossRef](#)]
9. Xia, F.F.; Jia, W.C.; Ma, C.Y.; Yang, R.; Wang, Y.; Potts, M. Synthesis and characterization of Ni-doped TiN thin films deposited by jet electrodeposition. *Appl. Surf. Sci.* **2018**, *434*, 228–233. [[CrossRef](#)]
10. Wu, M.; Jia, W.; Lv, P. Electrodepositing Ni-TiN nanocomposite layers with applying action of ultrasonic waves. *Procedia Eng.* **2017**, *174*, 717–723. [[CrossRef](#)]
11. Chen, Y.; Hao, Y.; Huang, W.; Ji, Y.; Yang, W.; Yin, X.; Liu, Y.; Ling, X. Corrosion behavior of Ni-P-nano-Al₂O₃ composite coating in the presence of anionic and cationic surfactants. *Surf. Coat. Technol.* **2017**, *310*, 122–128. [[CrossRef](#)]
12. Xu, Z.; Chen, Y. Characterization of nano-sized SiC-Ni composite fabricated by electroless plating method. *J. Nanosci. Nanotechnol.* **2013**, *13*, 1456–1460. [[CrossRef](#)] [[PubMed](#)]
13. Alizadeh, M.; Cheshmpish, A. Electrodeposition of Ni-Mo/Al₂O₃ nano-composite coatings at various deposition current densities. *Appl. Surf. Sci.* **2019**, *466*, 433–440. [[CrossRef](#)]
14. Youssef, K.; Koch, C.C.; Fedkiw, P.S. Improved corrosion behavior of nanocrystalline zinc produced by pulse-current electrodeposition. *Corros. Sci.* **2004**, *46*, 51–64. [[CrossRef](#)]
15. Santos, A.; Vojkuvka, L.; Pallarés, J.; Ferré-Borrull, J.; Marsal, L.F. Cobalt and nickel nanopillars on aluminium substrates by direct current electrodeposition process. *Nanoscale Res. Lett.* **2009**, *4*, 1021. [[CrossRef](#)]
16. Lee, D.B.; Ko, J.H.; Kwon, S.C. High temperature oxidation of Ni-W coatings electroplated on steel. *Mater. Sci. Eng. A* **2004**, *380*, 73–78. [[CrossRef](#)]
17. Hefnawy, A.; Elkhoshkhany, N.; Essam, A. Ni-TiN and Ni-Co-TiN composite coatings for corrosion protection: Fabrication and electrochemical characterization. *J. Alloys Compd.* **2018**, *735*, 600–606. [[CrossRef](#)]
18. Xia, F.; Jia, W.; Jiang, M.; Cui, W.; Wang, J. Microstructure and corrosion properties of Ni-TiN nanocoatings prepared by jet pulse electrodeposition. *Ceram. Int.* **2017**, *43*, 14623–14628. [[CrossRef](#)]
19. Li, X.; Feng, J.; Jiang, Y.; Lin, H.; Feng, J. Preparation and properties of TaSi₂-MoSi₂-ZrO₂-borosilicate glass coating on porous SiC ceramic composites for thermal protection. *Ceram. Int.* **2018**, *44*, 19143–19150. [[CrossRef](#)]
20. Sajjadnejad, M.; Omidvar, H.; Javanbakht, M. Influence of pulse operational parameters on pure nickel electrodeposits: Part II. Microhardness and corrosion resistance. *Surf. Eng.* **2017**, *33*, 94–101. [[CrossRef](#)]
21. Sajjadnejad, M.; Omidvar, H.; Javanbakht, M.; Mozafari, A. Textural and structural evolution of pulse electrodeposited Ni/diamond nanocomposite coatings. *J. Alloys Compd.* **2017**, *704*, 809–817. [[CrossRef](#)]
22. Xia, F.; Tian, J.; Ma, C.; Potts, M.; Guo, X. Effect of pulse frequency on microstructural, nanomechanical and wear properties of electrodeposited Ni-TiN composite coatings. *J. Appl. Phys.* **2014**, *116*, 234301–234306. [[CrossRef](#)]
23. Xia, F.; Tian, J.; Wang, W.; He, Y. Effect of plating parameters on the properties of pulse electrodeposited Ni-TiN thin films. *Ceram. Int.* **2016**, *42*, 13268–13272. [[CrossRef](#)]
24. Ma, C.; Jiang, M.; Xia, F. Preparation and characterization of Ni-TiN thin films electrodeposited with nickel baths of different TiN nanoparticle concentration. *Surf. Rev. Lett.* **2016**, *24*, 1750063. [[CrossRef](#)]
25. León-Patiño, C.A.; García-Guerra, J.; Aguilar-Reyes, E.A. Tribological characterization of heat-treated Ni-P and Ni-P-Al₂O₃ composite coatings by reciprocating sliding tests. *Wear* **2019**, *426–427*, 330–340. [[CrossRef](#)]
26. Mousavian, R.T.; Behnamfard, S.; Heidarzadeh, A.; Taherkhani, K.; Brabazon, D. Incorporation of SiC ceramic nanoparticles into the aluminum matrix by a novel method: Production of a metal matrix composite. *Met. Mater. Int.* **2021**, *27*, 2968–2976. [[CrossRef](#)]